# Sara Endosomes and the Maintenance of Dpp Signaling Levels Across Mitosis

Christian Bökel, *et al.*

*Science* **314**, 1135 (2006);
DOI: 10.1126/science.1132524



Science (print ISSN 0036-8075; online ISSN 1095-9203) is published weekly, except the last week in December, by the American Association for the Advancement of Science, 1200 New York Avenue NW, Washington, DC 20005. 

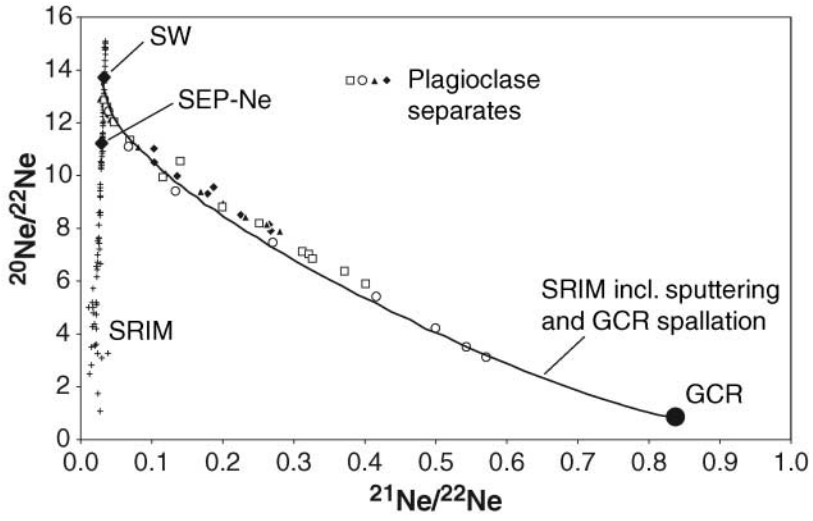


**Fig. 3.** Comparison of Ne data measured in plagioclase separates from several lunar soils by in vacuo etching (*10*) (squares, circles, triangles, and diamonds), with a simulated mixture of SW Ne fractionated as a function of implantation depth according to SRIM (crosses) and GCR-Ne, assuming SW sputter-saturation equilibrium (*16*). Surface sputtering shifts SRIM results to SW-like values for surface-sited Ne. Adding GCR-Ne moves the modeled data points to higher $^{21}Ne/^{22}Ne$ ratios, leading to a slightly curved line (solid line) that is hardly discernible from the straight line fit through the measured lunar data points for later steps (Fig. 1). Therefore, the lunar data are well reproduced by a SW and GCR mixture only, without an SEP-Ne component. This reflects the fact that the heavily fractionated solar Ne from the deepest layers (with $^{20}Ne/^{22}Ne$ value below that of SEP-Ne) is rare and hardly influences the mixing simulation. This strongly indicates that an independent component with the isotopic composition of SEP-Ne is not required to explain the lunar data.

tribution of solar energetic particles, now indicate a relative enrichment of (isotopically heavy) fractionated SW from greater depths due to, for example, the loss of outermost grain layers. Examples of this are $^{20}Ne/^{22}Ne$ ratios as low as ~11 in interplanetary dust particles (*6*). One may also speculate that the "Ne B" component in Earth's mantle proposed by (*26*, *27*) is possibly a result of a contribution of fractionated implanted SW-Ne during terrestrial accretion.

### References and Notes


1. J. Geiss *et al.*, *Space Sci. Rev.* **110**, 307 (2004).
2. J. F. Ziegler, *Nucl. Instrum. Methods Phys. Res. B* **219-220**, 1027 (2004).
3. J.-P. Benkert, H. Baur, P. Signer, R. Wieler, *J. Geophys. Res. (Planets)* **98**, 13147 (1993).
4. R. Wieler, H. Baur, P. Signer, *Geochim. Cosmochim. Acta* **50**, 1997 (1986).
5. A. S. Tamhane, J. K. Agrawal, *Earth Planet. Sci. Lett.* **42**, 243 (1979).
6. R. O. Pepin, R. L. Palma, D. J. Schlutter, *Meteorit. Planet. Sci.* **35**, 495 (2000).
7. P. Etique, P. Signer, R. Wieler, *Lunar Planet. Sci. Conf.* **XII**, 265 (1981).
8. D. C. Black, R. O. Pepin, *Earth Planet. Sci. Lett.* **6**, 395 (1969).
9. D. C. Black, *Geochim. Cosmochim. Acta* **36**, 347 (1972).
10. R. Wieler, *Space Sci. Rev.* **85**, 303 (1998).
11. W. F. Dietrich, J. A. Simpson, *Astrophys. J.* **231**, L91 (1979).
12. R. A. Mewaldt, J. D. Spalding, E. C. Stone, *Astrophys. J.* **280**, 892 (1984).
13. R. A. Mewaldt, R. C. Ogliore, G. Gloeckler, G. M. Mason, in *Solar and Galactic Composition*, *AIP Conference Proceedings*, R. F. Wimmer-Schweingruber, Ed. (American Institute of Physics, Melville, NY, 2001), vol. 598, pp. 393–398.
14. R. A. Leske *et al.*, *Cosmic Ray Conf.* **XXVIII**, 3237 (2003).
15. R. F. Wimmer-Schweingruber, P. Bochsler, in *Solar and Galactic Composition*, *AIP Conference Proceedings*, R. F. Wimmer-Schweingruber, Ed. (American Institute of Physics, Melville, NY, 2001), vol. 598, pp. 399–404.
16. Material, methods, and data are available as supporting material on *Science* Online.
17. A. J. G. Jurewicz *et al.*, *Space Sci. Rev.* **105**, 535 (2003).
18. D. S. Burnett *et al.*, *Space Sci. Rev.* **105**, 509 (2003).
19. V. Heber, thesis 14579, ETH Zürich (2002), http://e-collection.ethbib.ethz.ch/show?type=diss&nr=14579.
20. R. C. Reedy, *Lunar Planet. Sci. Conf.* **XXXVII**, abstract 1419 (2006) (CD-ROM).
21. R. H. Becker, *Lunar Planet. Sci. Conf.* **XXIX**, abstract 1329 (1998) (CD-ROM).
22. I. Leya, H.-J. Lange, S. Neumann, R. Wieler, R. Michel, *Meteorit. Planet. Sci.* **35**, 259 (2000).
23. R. O. Pepin, R. H. Becker, D. J. Schlutter, *Geochim. Cosmochim. Acta* **63**, 2145 (1999).
24. K. Hashizume, M. Chaussidon, *Nature* **434**, 619 (2005).
25. K. J. Mathew, J. F. Kerridge, K. Marti, *Geophys. Res. Lett.* **25**, 4293 (1998).
26. C. J. Ballentine, B. Marty, B. S. Lollar, M. Cassidy, *Nature* **433**, 33 (2005).
27. M. Trieloff, J. Kunz, D. A. Clague, D. Harrison, C. J. Allègre, *Science* **288**, 1036 (2000).
28. R. C. Wiens, P. Bochsler, D. S. Burnett, R. F. Wimmer-Schweingruber, *Earth Planet. Sci. Lett.* **226**, 549 (2004).
29. D. B. Reisenfeld *et al.*, paper presented at the 37th Lunar and Planetary Science Conference, Houston, TX, 14 March 2006.


30. The BMG experiment was made possible by the support of the entire Genesis Project at the Jet Propulsion Laboratory (JPL), Los Alamos National Laboratory, and Lockheed Martin, with special thanks to the JPL Genesis Canister design team, headed by D. Sevilla, and to the Genesis curation team at Johnson Space Center. We also thank I. Leya for constructive comments and suggestions, O. J. Homan for plasma-cleaning the BMG, and S. Tosatti for nondestructive x-ray photoelectron spectroscopy surface analyses. This study was financially supported by the Swiss National Science Foundation and the Genesis Project.


### Supporting Online Material

www.sciencemag.org/cgi/content/full/314/5802/1133/DC1
Materials and Methods
Fig. S1
Tables S1 and S2
References and Notes

7 August 2006; accepted 4 October 2006
10.1126/science.1133568

# Sara Endosomes and the Maintenance of Dpp Signaling Levels Across Mitosis

**Christian Bökel,[1]* Anja Schwabedissen,[1] Eugeni Entchev,[1] Olivier Renaud,[1]† Marcos González-Gaitán[1,2]‡**

During development, cells acquire positional information by reading the concentration of morphogens. In the developing fly wing, a gradient of the transforming growth factor–β (TGF-β)–type morphogen decapentaplegic (Dpp) is transduced into a gradient of concentration of the phosphorylated form of the R-Smad transcription factor Mad. The endosomal protein Sara (Smad anchor for receptor activation) recruits R-Smads for phosphorylation by the type I TGF-β receptor. We found that Sara, Dpp, and its type I receptor Thickveins were targeted to a subpopulation of apical endosomes in the developing wing epithelial cells. During mitosis, the Sara endosomes and the receptors therein associated with the spindle machinery to segregate into the two daughter cells. Daughter cells thereby inherited equal amounts of signaling molecules and thus retained the Dpp signaling levels of the mother cell.

In recent years, it has become clear that trafficking through the endosomal pathway is intimately linked with the emission, dispersion, and transduction of intercellular signals during development (*1*). In particular, the endosomal adaptor protein Sara (Smad anchor for receptor activation) plays a key role during transforming growth factor–β (TGF-β) signal transduction (*2*). To study the role of Sara during development, we first determined the

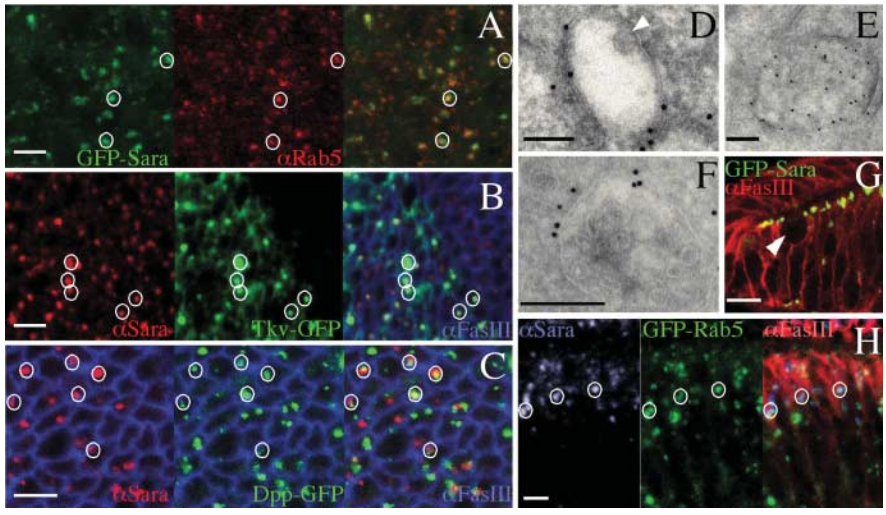


**Fig. 1.** Sara endosomes in interphase cells. (**A** to **C**) Apical XY confocal sections through imaginal disc cells. (A) Colocalization between Sara endosomes (GFP-Sara, green) and Rab5 (red). [(B) and (C)] Endogenous Sara (red) colocalizes with Tkv-GFP [(B), green] or GFP-Dpp [(C), green]. Cells were outlined by means of FasIII immunostaining (blue). 5.8 ± 0.7% of the total Tkv-GFP is in Sara endosomes and the rest is at the plasma membrane and other vesicular structures (fig. S13C). (**D** to **F**) MVE localization of Tkv-GFP [(D) and (E)] and GFP-Sara (F) with antibodies to GFP in cryoimmunoelectron micrographs. Tkv-GFP is detected at the limiting membrane of an early MVE [(D); arrowhead indicates an invaginating internal vesicle] and at both the limiting membrane and internal vesicles in a mature MVE (E). GFP-Sara is exclusively found at the limiting membrane (F). (**G** and **H**) Z wing cryosections reveal tight apical localization of Sara endosomes [GFP-Sara, (G), green; GFP-Rab5, (H), green; endogenous Sara, (H), blue; FasIII, red]. There is an absence of Sara from more basal Rab5 endosomes (H). Arrowhead in (G) indicates a dividing cell. Examples for colocalization of GFP-tagged Dpp, Tkv, and Rab5 with Sara endosomes are highlighted by white circles in (A) to (C) and (H). Scale bars, 2 μm in (A) to (C) and (H), 100 nm in (D) to (F), and 5 μm in (G).

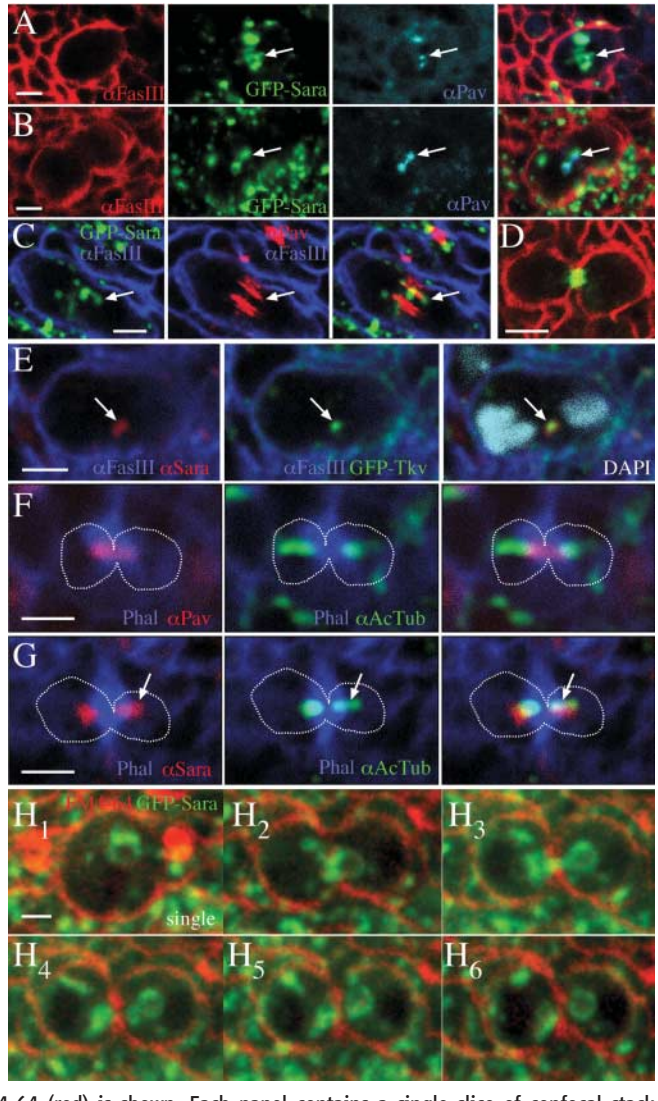


**Fig. 2.** Sara endosomes in dividing cells. (**A** to **D**) GFP-Sara (green) localizes to the central spindle (arrows) marked by Pavarotti [(A) and (B), blue; (C), red] at progressive stages of mitosis [(A), early anaphase; (C), late anaphase; (B), telophase; (D), cytokinesis] in dividing wing epithelial cells outlined with FasIII [(A), (B), and (D), red; (C), blue]. (**E**) A fraction of intracellular Tkv-GFP (green) colocalizes with endogenous Sara (red) at the cleavage plane (arrows). Cell was outlined by means of FasIII (blue) and DNA was marked by 4′,6′-diamidino-2-phenylindole (DAPI) (light blue). (**F** and **G**) Dividing wing cells stained for Pavarotti [(F), red] or Sara [(G), red], acetylated tubulin (green), and actin with the use of fluorescent phalloidin (blue). Acetylated tubulin appears in the midzone during telophase and surrounds the central spindle defined by Pavarotti (F). At this stage, the Sara endosomes colocalize with acetylated tubulin (G) and not with Pavarotti (arrows). Dotted lines indicate cell outlines. (**H**) Time lapse documenting the segregation of GFP-Sara (green) expressed at high levels. A dividing wing epithelial cell outlined by the lipid dye FM4-64 (red) is shown. Each panel contains a single slice of confocal stack centered on the cleavage site. Scale bars, 2 μm.

subcellular localization of Sara in developing wing epithelial cells in *Drosophila* (*3*). As in mammals (*2*, *4*), Sara in *Drosophila* wing disc cells accumulated at early endosomes. Sara colocalized with the early endosomal marker Rab5 (Fig. 1A and fig. S1E) and with fluorescent dextran internalized in a short pulse (fig. S1, A and E). In contrast, Sara endosomes did not colocalize with dextran after a 40-min chase (fig. S1, B and E). Furthermore, Sara was absent from Rab7-positive late endosomes and lysosomes and Rab11-positive recycling endosomes (fig. S1, C to E). Sara endosomes thus represent an early endosomal compartment.

Sara was targeted to phosphatidylinositol 3-phosphate [PI(3)P]–containing early endosomes via its PI(3)P-binding FYVE domain (figs. S1E and S2, A and B) (*2*) and colocalized with the FYVE-domain protein hepatocyte growth factor–regulated tyrosine kinase substrate (Hrs) (figs. S1E and S2D). Hrs itself colocalizes with early endosomes (*5*), where it initiates multivesicular endosome (MVE) biogenesis (*6*). Like Hrs (*7*) and other FYVE-domain proteins, Sara was found on the MVE-limiting membranes (Fig. 1F and fig. S11), although the internal vesicles show peak levels of PI(3)P (*8*). MVEs can be intermediates in the degradation pathway but have also been implicated in the recycling and storage of endocytic cargo (*9*). Indeed, Sara

[1]Max Planck Institute of Molecular Cell Biology and Genetics, Pfotenhauerstrasse 108, 01307 Dresden, Germany. [2]Department of Biochemistry and Department of Molecular Biology, Geneva University, Sciences II, 30 Quai Ernest-Ansermet, 1211 Geneva 4, Switzerland.

*Present address: Biotechnological Center, Dresden University of Technology, Tatzberg 47, 01307 Dresden, Germany.

†Present address: Automation Project, Plateforme d'Imagerie Dynamique, Institut Pasteur, 25–28, rue du Docteur Roux, 75015 Paris, France.

‡To whom correspondence should be addressed. E-mail: marcos.gonzalez@biochem.unige.ch

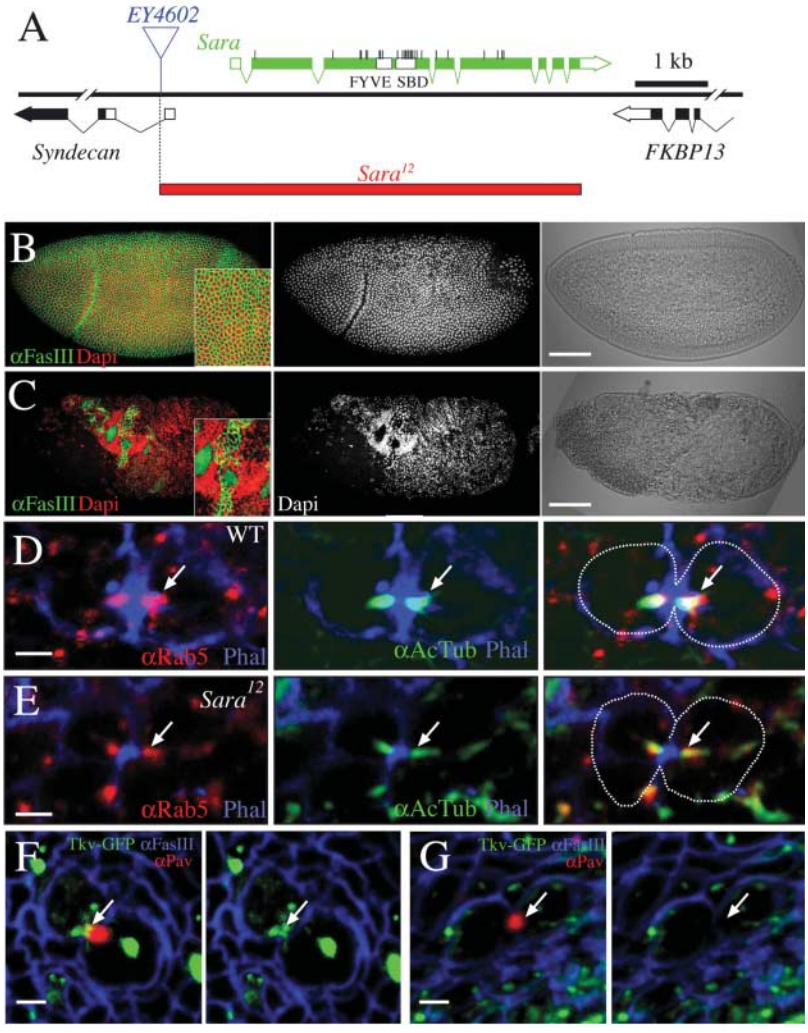


**Fig. 3.** Sara targets signaling cargo to the central spindle. (**A**) Genomic organization of *Sara* (transcript, green; open reading frame, solid green) and flanking genes (*FKBP13* and *Syndecan*). A transposable element EY4602 (blue) inserted in the first intron of *Syndecan* was used to generate a 5.8-kb deletion by imprecise excision ($sara^{12}$, red), which complements the loss-of-function *Syndecan* alleles. Amino acid exchanges in TILLING mutants, FYVE-, and Smad-binding domains (SBD) are indicated. (**B** and **C**) Double stainings of wild-type (WT) (B) and maternal/zygotic mutant $sara^{12}$ (C) embryos. Cell outlines were marked with FasIII (green) and nuclei were marked by DAPI (red, left panel; gray, center panel). Nomarski images appear in the right panel. High-magnification insets show local cellularization of $sara^{12}$ mutant embryos. The lower density of nuclei in the anterior part of the mutant embryo (C) uncovers a mitotic defect before cellularization. (**D** and **E**) Endogenous Rab5 (red) colocalizes (arrows) with spindle-acetylated tubulin (green) both in WT [(D), 91% of cells] and $sara^{12}$ [(E), 89% of cells] dividing wing disk cells outlined with fluorescent phalloidin (blue). Dotted lines indicate cell outlines. (**F** and **G**) Intracellular Tkv-GFP (green) associates with the midbody marked by Pavarotti (arrows, red) in WT [(F), 90% of cells] but not $sara^{12}$ mutant cells [(G), 10% of cells] outlined by means of FasIII immunostaining (blue). Levels of total Tkv in all endo- and exocytic subcellular compartments in the two daughter cells are approximately equal when the complete *z* axis is quantified (1.20 ± 0.28 ratio of Tkv levels in the sibling cells, $n = 13$ cell pairs; not significantly different from ratio = 1, $P > 0.531$), and overexpression levels do not differ between WT and mutant backgrounds (fig. S13E). Scale bars, 50 μm in (B) and (C) and 2 μm in (D) to (G).

endosomes correspond to a signaling compartment that segregates from the degradation pathway (*10*).

Sara has been implicated in TGF-β and decapentaplegic (Dpp) signal transduction (*2*, *4*, *11*). Consistently, Sara-positive endosomes contained Dpp and its receptor Thickveins (Tkv) (Fig. 1, B and C). Tkv was found at the limiting membrane of early MVEs and the internal vesicles of mature MVEs (Fig. 1, D and E, and fig. S11).

The Sara-positive endosomes were clustered in the top 3 μm of the 30-μm-tall columnar wing epithelium (Fig. 1G and fig. S3, A and C). More basal Rab5-positive early endosomes lacked Sara (Fig. 1H and fig. S3, B and C). In total, only 12% of the Rab5 endosomes were Sara-positive. Thus, Sara defined a strictly apical subpopulation of early endosomes confined to a small volume representing the top 10% of each cell (fig. S3A). We wondered how the mother cells ensure that this polarized compartment and its cargo are partitioned to each daughter cell during mitosis.

Dividing wing cells rounded up at the apical surface of the epithelium during prophase (Fig. 1G). At anaphase, Sara was targeted to the mitotic spindle midzone (also called the central spindle) as monitored by immunostaining with the centraspindlin kinesin Pavarotti/kinesin-like protein–1 (*12*) (Fig. 2, A to C). These Sara-positive structures corresponded to endosomal compartments as they colocalized with internalized dextran and the endosomal markers Rab5 and green fluorescent protein (GFP) fused to a tandem FYVE domain (2xFYVE-GFP) (fig. S4). Furthermore, Sara-positive endosomes at the cleavage plane contained the transmembrane receptor Tkv (Fig. 2E). Later during cytokinesis, the Sara endosomes were displaced off the Pavarotti-positive central spindle and colocalized with acetylated tubulin at both ends of the central spindle (Fig. 2, F and G). In this way, the pool of Sara endosomes targeted to the center of the cell was partitioned into two subpopulations, which then segregated into the two daughter cells. After mitosis, the Sara compartments remained associated with the midbody at the apical side of the epithelial cells (Fig. 2, D and H), which then regained their columnar aspect.

Other endosomal structures, such as lysosomes and late endosomes, did not associate with the spindle but were randomly segregated during mitosis (fig. S5A). Rab11-positive recycling endosomes associate with the centrosomes during cytokinesis (*13*, *14*) (fig. S5B). In the case of Rab5-positive early endosomes, one subset segregated randomly, whereas another population potentially corresponding to the Sara endosomes associated with the central spindle (Fig. 3D and figs. S4B and S5C).

In order to analyze the role of Sara in endosomal or cargo targeting to the central spindle, we generated *Sara* deletions. $sara^{12}$ removes the entire Sara coding region and represents a null mutation (Fig. 3A and fig. S12D). Zygotic $sara^{12}$ mutants died during late larval and pupal development. In rare cases (5%), they survived until adulthood, showing variable vein defects (Fig. 4, L to Q). Most maternal/zygotic $sara^{12}$ mutants (92.2%) died during embryogenesis with erratic phenotypes, including cellularization and dorsal/ventral patterning defects among others (Fig. 3, B and C). Few animals (1.4%; $n = 1520$) reached the third instar larval stage. Both Mad phosphorylation and the pattern of the Dpp target gene *spalt* were normal in the absence of Sara (figs. S10 and S12). Thus, although Sara is essential for activin/TGF-β signaling by recruiting Smad2/3 to the receptor complex for

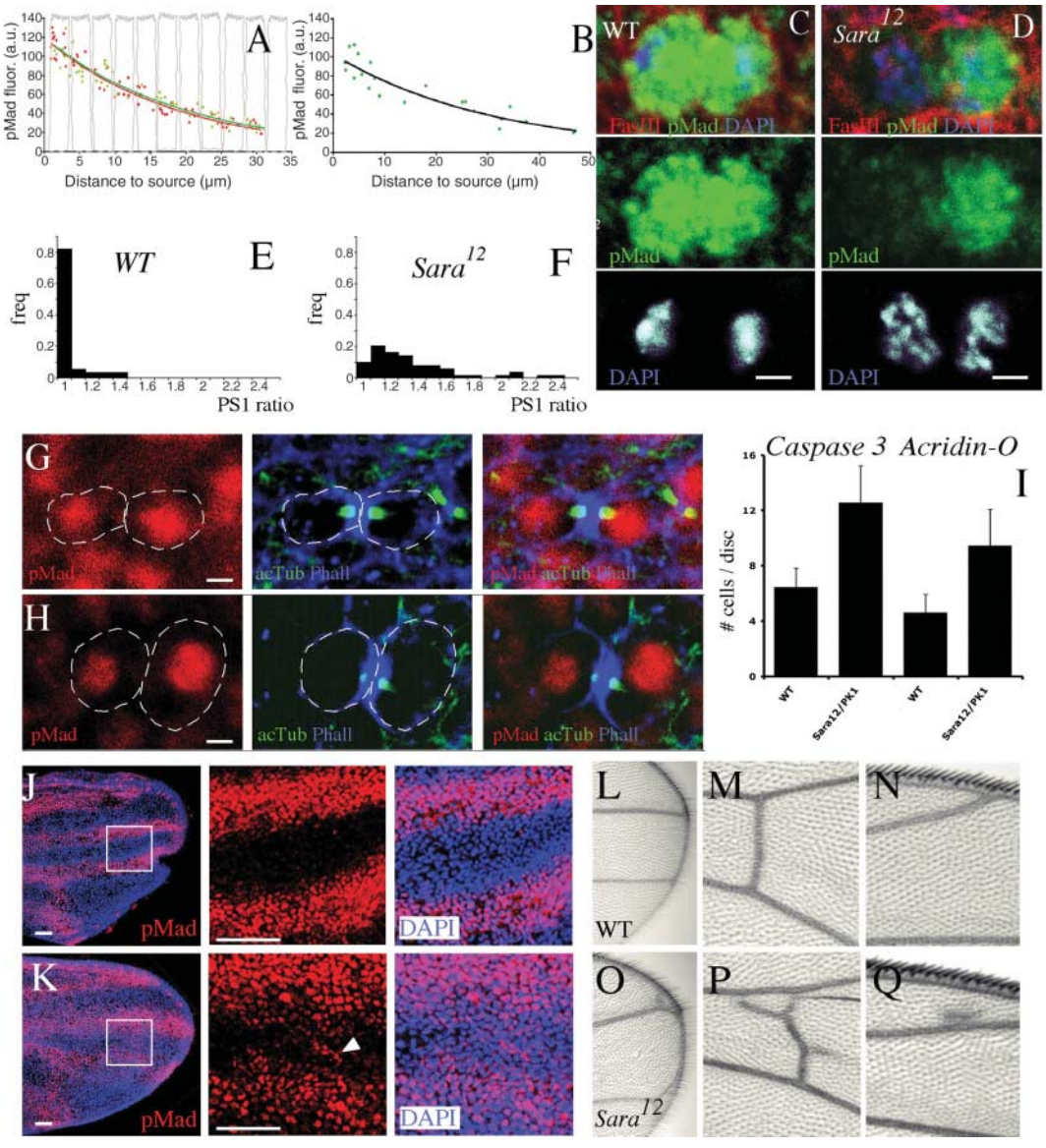


**Fig. 4.** Sara maintains Dpp signaling levels across mitosis. (**A**) Normalized pMad immunofluorescence intensity in individual cells plotted against the distance from Dpp source. a.u., arbitrary units. Cell outlines correspond to average actual dimensions. The different colors and symbols denote individual disks. (**B**) Normalized pMad signal in mitotic cells versus distance from Dpp source. Although absolute pMad levels are about 10-fold increased relative to interphase, a regular gradient is retained ($n$ = 3 discs). (**C** and **D**) pMad staining (green) in WT (C) and *sara*$^{12}$ mutant sibling cell pairs (D) at the exit of mitosis, counterstained with FasIII (red) and DAPI (blue). Compare equal pMad levels in the WT sibling cells (C) with unequal pMad levels in the mutant (D). (**E** and **F**) Ratios of pMad signals in WT (E) and *sara*$^{12}$ (F) pairs of sibling cells ($n$ = 60 pairs per genotype) at the exit of mitosis. (**G** and **H**) Dividing cells of WT (G) and *sara*$^{12}$/Df(2R)PK1 (H) pupal wings in 17 hours after puparium formation (apf). Sibling pairs are identified by the accumulation of actin (fluorescent phalloidin, blue) and acetylated tubulin (green) at the contact site. Dashed lines indicate cell outlines. Ratios of pMad (red) intensity between sibling cells are 1.09 for the WT (G) and 2.07 for the mutant pair (H). (**I**) Quantification of apoptosis levels in WT and *sara*$^{12}$/Df(2R)PK1 wing disks via caspase-3 immunostaining and acridin orange staining. Differences were significant ($P$ < 0.001). Error bars indicate SD. (**J** and **K**) WT (J) and *sara*$^{12}$/Df(2R)PK1 (K) wings 25 hours apf, stained for pMad (red). Nuclei were marked with DAPI (blue). pMad activation defines the presumptive vein territories, but ectopic pMad (arrowhead) appears in the intervein territory of the mutant wing (center and right panels are magnifications of the boxed areas in the left panels). (**L** to **Q**) *sara*$^{12}$ mutant flies [(O) to (Q)], but not WT control flies [(L) to (N)], exhibit delta formation at vein junctions with the margin [(L) and (O), 85% of mutant wings], branching of the posterior cross-vein [(M) and (P), 28%], and partial vein duplications [(N) and (Q), 15%]. Scale bars, 2 μm in (C), (D), (G), and (H) and 20 μm in (J) and (K).

phosphorylation (*2*, *4*), it is not required in the same way for Dpp/bone morphogenetic protein signal transduction.

We also generated 32 Sara point mutations (Fig. 3A) in two targeted induction of lesions in large genomes (TILLING) reverse genetic screens (*15*). These mutations included *sara*$^{1}$, a Met$^{538}$→Lys$^{538}$ amino acid exchange in a conserved position of the FYVE domain that mistargets Sara out of the apical endosomes into the cytosol (fig. S2, E and F). Both *sara*$^{12}$ and *sara*$^{1}$ were lethal mutations sharing phenotypes described below (fig. S6). Both phenotype and lethality could be rescued by expressing a Sara transgene under the tubulin promotor or the GFP-Sara fusion by means of the Gal4 system (table S1 and fig. S7). Thus, the defects described were caused by impaired Sara function, and GFP-Sara was functional.

In both *sara*$^{1}$ and *sara*$^{12}$ zygotic mutants, targeting of endosomes to the central spindle is normal (Fig. 3, D and E, and fig. S8). However, Tkv failed to localize to the central spindle (Fig. 3, F and G, and fig. S13, A, B, and D). Thus, Sara is involved in targeting signaling cargo to endosomes associated with the spindle machinery.

To test whether this biological function of Sara was functionally relevant for Dpp signaling, we quantified Mad phosphorylation in interphase cells and twin daughter cells after cell division. In wild-type wings, phosphorylated Mad (pMad) in interphase cells forms a single exponential concentration gradient profile that parallels the Dpp gradient (*16*): Over a range of 30 μm (~10 cell diameters), the levels of nuclear pMad phosphorylation decayed by a factor of 6 (Fig. 4A and fig. S10). This pMad gradient is thought to encode the anterior/posterior positional information in the disk (*16*).

Mitotic cells showed 10-fold higher levels of Mad phosphorylation than surrounding interphase cells (fig. S9) but retained a pMad gradient profile (Fig. 4B). After mitosis, wild-type twin daughter cells that were identified morphologically or by molecular markers reliably showed equal levels of pMad both in the wing disk (Fig. 4, C and E and fig. S14, B and D) and in pupal wings (Fig. 4G and fig. S15A). In contrast, mutant *sara*$^{12}$ twin daughter cells showed a high variability in pMad levels, reaching up to 2.5-fold

between the twin daughter cells (Fig. 4, D, F, and H, and figs. S14, C and D, and S15B), corresponding to a positional information distance of up to six cells (or 20 μm) (Fig. 4A). Distribution of nonphosphorylated Mad was not affected (fig. S13F). Thus, Sara endosomes store signaling molecules (receptors and/or transcription factors) and are partitioned into the twin daughter cells by association with the central spindle. Sara itself is required for central spindle targeting of the receptor cargo and ensures the maintenance of the levels of pMad within the gradient across mitosis.

The differences in pMad levels between twin sibling cells decrease with time after mitosis in Sara mutants, leading to an overall normal pMad gradient with normal amplitude and range in interphase cells (fig. S10). Consistently, wings of *sara*$^{12}$ escapers did not exhibit large-scale Dpp-related patterning phenotypes (Fig. 4, L to Q). This result implies the existence of mechanisms that smooth the uneven signaling levels in Sara mutants after mitosis. These mechanisms may include the elimination of cells causing discontinuities in the pMad gradient by *brinker*-mediated apoptosis (*17*). Correspondingly, elevated apoptosis levels were observed both in Sara mutant wings (Fig. 4I and fig. S16, B, C, and E) and in Sara mutant clones relative to the surrounding tissue (fig. S16, A and D). Cells entering apoptosis, as monitored by the expression of head involution defective (Hid), exhibited elevated pMad levels in comparison with their neighbors (fig. S16F), which is consistent with previous observations (*18*, *19*). In contrast, daughter cells with inappropriately low signaling levels after mitosis appeared to recover in interphase, implying that, in the larval disk, there is time for de novo signaling by the extracellular gradient of Dpp before cells are committed to a specific fate.

Uneven signaling levels after mitosis should become fixed if differentiation occurred right after division. In the pupal wing, Dpp signaling involved in the determination of vein versus intervein tissue coincides with the final mitotic wave (*20*, *21*). Consistently, we observed cells with ectopically elevated Dpp signaling levels in the intervein territory of Sara mutant wings but not wild-type wings (Fig. 4, J and K), as well as corresponding morphological defects such as branching or partial duplication (Fig. 4, L to Q).

Why do daughter cells retain the Dpp signaling levels of their mother across mitosis, if they are able to read the extracellular gradient of Dpp again after division? We speculate that our observations might be related to the phenomenon of cellular memory of activin signaling in *Xenopus*, where cells remember activation levels for 3 to 6 hours (even across mitosis) (*22*, *23*) because of the retention of activated receptors within the endocytic pathway (*24*). Dpp signaling in flies does not show long-term memory over several cell generations (*25*). However, Dpp signaling may well exhibit short-term memory of a few hours, which would buffer against signaling fluctuations. Uneven distribution of signaling molecules during mitosis (as in Sara mutants) would then generate a situation in which one of the daughter cells may exhibit signaling levels above the levels corresponding to its actual position. Such discontinuities compromise the robustness of the interpretation of the gradient but will to some extent be compensated by *brinker*-dependent apoptosis (*17*). Our observations thus imply a double mechanism to ensure robustness in the interpretation of the gradient: first, error prevention by preempting the appearance of discontinuities after mitosis through Sara and then, should discontinuities appear, error correction through proofreading and apoptosis (*17*, *18*).

### References and Notes


1. M. Gonzalez-Gaitan, *Nat. Rev. Mol. Cell Biol.* **4**, 213 (2003).
2. T. Tsukazaki, T. A. Chiang, A. F. Davison, L. Attisano, J. L. Wrana, *Cell* **95**, 779 (1998).
3. Materials and methods are available as supporting material on *Science* Online.
4. E. Panopoulou *et al.*, *J. Biol. Chem.* **277**, 18046 (2002).
5. C. Raiborg, K. G. Bache, A. Mehlum, E. Stang, H. Stenmark, *EMBO J.* **20**, 5008 (2001).
6. D. J. Katzmann, C. J. Stefan, M. Babst, S. D. Emr, *J. Cell Biol.* **162**, 413 (2003).
7. M. Sachse, S. Urbe, V. Oorschot, G. J. Strous, J. Klumperman, *Mol. Biol. Cell* **13**, 1313 (2002).
8. D. J. Gillooly *et al.*, *EMBO J.* **19**, 4577 (2000).
9. J. Gruenberg, H. Stenmark, *Nat. Rev. Mol. Cell Biol.* **5**, 317 (2004).
10. G. M. Di Guglielmo, C. Le Roy, A. F. Goodfellow, J. L. Wrana, *Nat. Cell Biol.* **5**, 410 (2003).
11. D. Bennett, L. Alphey, *Nat. Genet.* **31**, 419 (2002).
12. R. R. Adams, A. A. Tavares, A. Salzberg, H. J. Bellen, D. M. Glover, *Genes Dev.* **12**, 1483 (1998).
13. G. Emery *et al.*, *Cell* **122**, 763 (2005).
14. B. Riggs *et al.*, *J. Cell Biol.* **163**, 143 (2003).
15. S. Winkler *et al.*, *Genome Res.* **15**, 718 (2005).
16. A. A. Teleman, S. M. Cohen, *Cell* **103**, 971 (2000).
17. E. Moreno, K. Basler, G. Morata, *Nature* **416**, 755 (2002).
18. T. Adachi-Yamada, M. B. O'Connor, *Dev. Biol.* **251**, 74 (2002).
19. A. Perez-Garijo, F. A. Martin, G. Morata, *Development* **131**, 5591 (2004).
20. J. F. de Celis, *Development* **124**, 1007 (1997).
21. M. Milan, S. Campuzano, A. Garcia-Bellido, *Proc. Natl. Acad. Sci. U.S.A.* **93**, 11687 (1996).
22. P. Y. Bourillot, N. Garrett, J. B. Gurdon, *Development* **129**, 2167 (2002).
23. S. Dyson, J. B. Gurdon, *Cell* **93**, 557 (1998).
24. J. Jullien, J. Gurdon, *Genes Dev.* **19**, 2682 (2005).
25. K. Weigmann, S. M. Cohen, *Development* **126**, 3823 (1999).


26. We thank C. P. Heisenberg, M. Zerial, and C. Gonzalez for comments on the manuscript; D. Backasch for excellent technical assistance; M. Wilsch-Braeuninger for help with electron microscopy; S. Winkler for her work on TILLING; and D. Glover, H. Bellen, and H. Steller for the Pavarotti, Hrs, and Hid antisera, respectively. This work was supported by the Max Planck Society, Human Frontier Science Program, Deutsche Forschungsgemeinschaft, and Volkswagen foundation.


### Supporting Online Material

www.sciencemag.org/cgi/content/full/314/5802/1135/DC1
Materials and Methods
SOM Text
Figs. S1 to S16
Table S1
References

14 July 2006; accepted 19 September 2006
10.1126/science.1132524

# Abortive Initiation and Productive Initiation by RNA Polymerase Involve DNA Scrunching

**Andrey Revyakin,[1,2]* Chenyu Liu,[1,2,3] Richard H. Ebright,[1]† Terence R. Strick[2,3]†**

**Using single-molecule DNA nanomanipulation, we show that abortive initiation involves DNA "scrunching"—in which RNA polymerase (RNAP) remains stationary and unwinds and pulls downstream DNA into itself—and that scrunching requires RNA synthesis and depends on RNA length. We show further that promoter escape involves scrunching, and that scrunching occurs in most or all instances of promoter escape. Our results support the existence of an obligatory stressed intermediate, with approximately one turn of additional DNA unwinding, in escape and are consistent with the proposal that stress in this intermediate provides the driving force to break RNAP-promoter and RNAP-initiation-factor interactions in escape.**

Transcription initiation involves a series of reactions (*1*–*3*). RNA polymerase (RNAP) binds to promoter DNA to yield an RNAP-promoter closed complex ($RP_c$). RNAP then unwinds ~1 turn of DNA surrounding the transcription start site to yield an RNAP-promoter open complex ($RP_o$). RNAP then enters into abortive cycles of synthesis and release of short RNA products as an RNAP-promoter initial transcribing complex ($RP_{itc}$) and, upon synthesis of an RNA product ~9 to 11 nucleotides (nt) in length, escapes the promoter and enters into productive synthesis of RNA as an RNAP-DNA elongation complex ($RD_e$).

The mechanism by which the RNAP active center translocates in abortive initiation and promoter escape has remained unclear. It has remained unclear because of two seemingly contradictory observations. First, RNA products up to ~8 to 10 nt in length are synthesized in